Journal of Organic Chemistry **2020**, *85*, 13747-13756

https://doi.org/10.1021/acs.joc.0c01882

Catalytic Synthesis of Luminescent Pyrimidines via Acceptorless Dehydrogenative Coupling

Rajarshi Mondal, Issiah B. Lozada, Olha Stotska and David E. Herbert*

Department of Chemistry and the Manitoba Institute for Materials
University of Manitoba, 144 Dysart Road, Winnipeg, Manitoba, R3T 2N2, Canada

*david.herbert@umanitoba.ca

ABSTRACT

A simple catalytic synthesis of luminescent pyrimidines from benzamidines and alcohols is reported. These one-pot, acceptorless dehydrogenative coupling reactions are catalyzed by a ruthenium hydrido chloride complex (**1**), supported by a chelating *P^N* ligand (**L1**) bearing a benzannulated phenanthridine donor arm. The pyrimidines thus produced are emissive in solution, with photoluminescence quantum yields (PLQY) reaching 72%. Details of the catalytic synthesis and characterization of the pyrimidines in both solution and the solid-state is reported, along with computational modelling of the emissive excited states of representative examples.

INTRODUCTION

Pyrimidines, long recognized for their critical role in biological processes,[1] have been increasingly considered for applications in medicinal chemistry[2,3] and as photo-emissive materials.[4] With respect to their photophysical properties, thanks to the presence of two electronegative nitrogen atoms, pyrimidines can serve as the electron-withdrawing core of donor-acceptor-donor (D–A–D) or donor-acceptor-acceptor (D-A-A) triads, or as a terminus in asymmetric (D–A) variants.[5] In these systems, the pyrimidine unit stabilizes the lowest unoccupied molecular orbital (LUMO), helping to facilitate charge-transfer within the molecule and enable their use as electron transport materials.[6] Such push-pull molecules are also sought as low band-gap materials for applications including light emitting diodes (LEDs),[7] photovoltaic devices[8–10] and organic electronics.[11]

As with emissive molecule design in general, there has been expanded interest of late in straightforward and more sustainable preparatory routes to highly substituted, emissive pyrimidines. Moving away from metal-catalyzed cross-coupling methodologies for the derivatization of halogenated pyrimidines,[12–19] for example, would obviate the production of halogenated waste. One-pot, coupling-isomerization sequences[20] and modified Pinner condensations involving silylated amidines[21] have been reported but similarly require functionalized precursors. In comparison, acceptorless dehydrogenative coupling (ADC) reactions of alcohols in the presence of benzamidine nucleophiles, variants of the so-called "indirect" Friedländer annulation,[22] employ a single catalyst for both the oxidation of alcohols and their catalytic condensation with amidines. They can thus be used to prepare a variety of highly substituted pyrimidines with only hydrogen gas and water as byproducts.[23–29] We herein report the application of this synthetic methodology for the preparation of a series of emissive, push-pull

pyrimidines (Figure 1). In addition to the catalytic preparation and full characterization of a series of novel pyrimidines, we furthermore describe their optical properties, along with computational modelling and solid-state structures of selected representatives, demonstrating the utility of ADC pathways for the preparation of asymmetric D-A-D' and D-A-A pyrimidine π-systems.

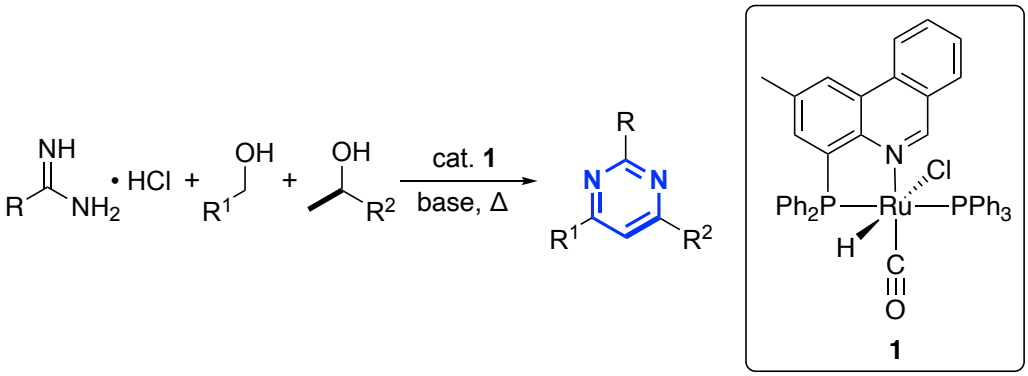

Figure 1. Multi-component synthesis of pyrimidines (core structure highlighted in blue) catalyzed by **1**.

RESULTS AND DISCUSSION:

While a number of catalytic routes to polysubstituted pyridines and quinolines via ADC mechanisms have been reported, only a limited number of homogeneous systems capable of the construction of pyrimidines have been disclosed.[23–28] We recently described the preparation and reactivity of a ruthenium hydrido chloride complex (**1**) supported by a simple, heteroleptic bidentate *P^N* ligand containing a diarylphosphine and a benzannulated phenanthridine donor arm.[30] In the presence of base, complex **1** efficiently catalyzes multi-component reactions using alcohol precursors to produce structurally diverse molecules including pyridines and quinolines. Notably, the ligand manifold in **1** does not bear readily (de)protonated Brønsted acidic or basic

groups common to transition metal catalysts capable of these sorts of transformations, suggesting metal-ligand cooperativity does not play a significant role in the catalytic ADC-type reactivity of **1**. Instead, formation of relatively stable and isolable η^2-aldehyde adducts are proposed to promote multicomponent reactions.

In that work, we also described the utility of **1** in the preparation of a limited selection of highly substituted pyrimidines in a one-pot ADC of benzamidine hydrochlorides, secondary alcohols and primary alcohols. Here, we extend this synthetic methodology to asymmetric emissive analogs (Table 1). Using previously optimized reaction conditions,[30] benzamidine hydrochloride, a secondary alcohol and a primary alcohol were combined with 0.5 mol % of **1** in the presence of a base (KO*t*Bu) and heated in an open reflux in dry toluene for 24 h. In this way, a library of 17 novel emissive pyrimidines (**P1-4**) was prepared. The catalysis tolerates inclusion of a methyl substituent at the *para*-position of the benzamidine precursor, which can furthermore be used as its more conveniently handled hydrochloride salt when an extra equivalent of base is introduced. The reaction conditions similarly tolerate a variety of functionalized alcohols, including those bearing methoxy, dimethyl and diphenyl amino, thiophene and terthiophene substituents, as well as carbazoles and extended pyrenyl and anthracenyl π-systems. For the secondary alcohols, slightly higher yields were observed with electron-poor biphenyl derivatized precursors compared with electron-rich methoxynapthyls. In terms of primary alcohols, the presence of electron-rich donor functionalities as in **P2f** led to moderately higher isolated yields. While the yields are fair to moderate, the pyrimidines are easily isolated in their pure forms following column chromatography on silica, including on larger, millimolar scales (see Experimental Section). Notably, asymmetric D-A-D' and D-A-A systems could be produced in one pot without requiring multi-step sequences of the sort common in the literature.[31]

Table 1. Preparation of emissive pyrimidines **P1-4** via acceptorless dehydrogenative coupling catalyzed by **1**.

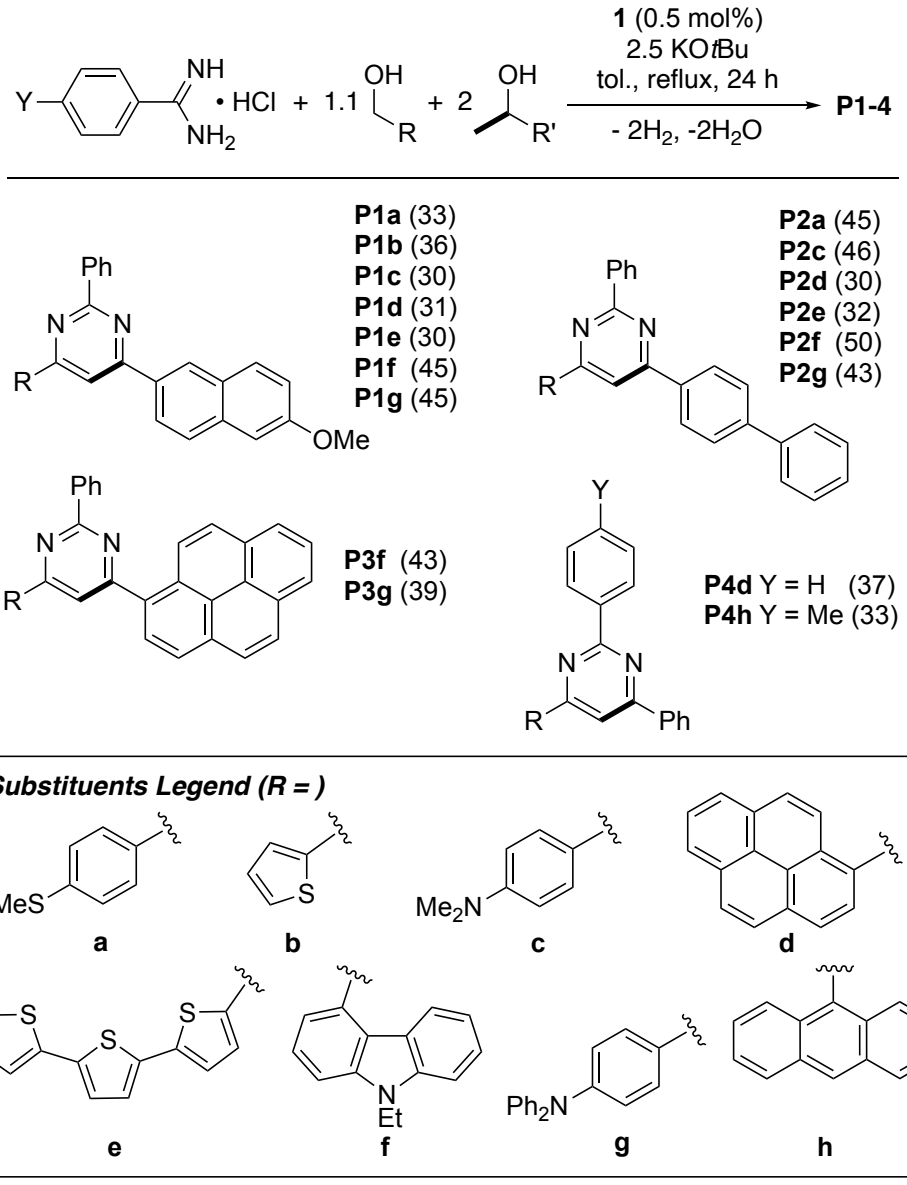

The pyrimidines thus produced were characterized in solution using both ^{1}H and ^{13}C NMR, with the exception of the terthiophene-substituted **P1e** for which a meaningful ^{13}C NMR spectrum could not be obtained due to poor solubility. In each case, formation of the central pyrimidine core was confirmed by observation of a distinctive singlet C*H* resonance in the aromatic region of the ^{1}H NMR spectrum just downfield of 8 ppm. High-resolution mass spectrometry (HRMS) was

further used to establish product identity. To confirm the solution-state connectivity, solid-state structures for two (*para*-amino)phenyl-substituted products, **P1c** and **P3g**, were obtained using single-crystal X-ray diffraction (Figure S1). The formation of the [N_2C_4] ring is readily apparent and its aromatic character can be deduced from the shorter C-C bond distances within the ring [C2-C3 **P1c**: 1.3923(18) Å, **P3g**: 1.386(2) Å; C3-C4 **P1c**: 1.3932(18) Å, **P3g**: 1.390(2) Å] compared with the adjoining exocyclic C-C bonds [C2-C19 **P1c**: 1.4807(18) Å, **P3g**: 1.484(2) Å; C4-C11 **P1c**: 1.4719(18) Å, **P3g**: 1.476(2) Å]. In the solid-state, the phenyl (15°) and naphthyl (38°) substituents of **P1g** are twisted with respect to the plane of the pyrimidine core. In **P3g**, the corresponding values are phenyl (21°) and pyrenyl (52°). The *para*-dimethylamino unit, however, is nearly planar in **P1g** with a sum of bond angles about N3 of 357°. In **P3g**, the corresponding sum of bond angles about the N3 of the diphenylamino unit (360°) is similarly indicative of conjugation of the amino lone pair into the pyrimidine acceptor core.

The mechanism of formation of **P1-4** is anticipated to mirror that involved in the catalytic formation of non-emissive analogs mediated by **1**,[30] which shows key differences from ADC-type mechanisms for pyrimidine formation catalyzed by other transition metal complexes, namely in the lack of observation of unsaturated chalcone intermediates proposed to play a central role in the formation of pyrimidines from alcohols.[29,26] While related catalysts based on Mn have been demonstrated to effectively catalyze one-pot, four-component reactions in which β-alkylation of a secondary alcohol by a primary alcohol is followed by addition of a different primary alcohol and an amidine to produce even more complex pyrimidines,[25] we have so far been unable to access similar reactivity with **1**.

Absorption and Emission Spectra

Pyrimidines **P1-4** were next characterized by steady-state absorption and emission spectroscopy in air-saturated CH_2Cl_2 solutions at 298 K. The pertinent photophysical data is shown in Figures 2-3 and summarized in Table 2. In solution, all 17 pyrimidines absorb strongly in the UV region; only the lowest energy absorption manifold of **P1e** and **P2e** extend meaningfully into the visible. For the most part, the absorption profiles are broad and featureless. The exception is the anthracenyl-bearing **P4h** (Figure 3b) which shows vibrational sub-levels with frequency differences between the sublevels of 1341 cm^{-1} and 1405 cm^{-1}, consistent with those found in anthracene itself.[32] Thus, for **P4h** electronic excitation between 349-386 nm results in population of anthracene π*-orbitals. Otherwise, the absorption profiles are unremarkable compared to those reported for other pyrimidine-based dyes.[19,33]

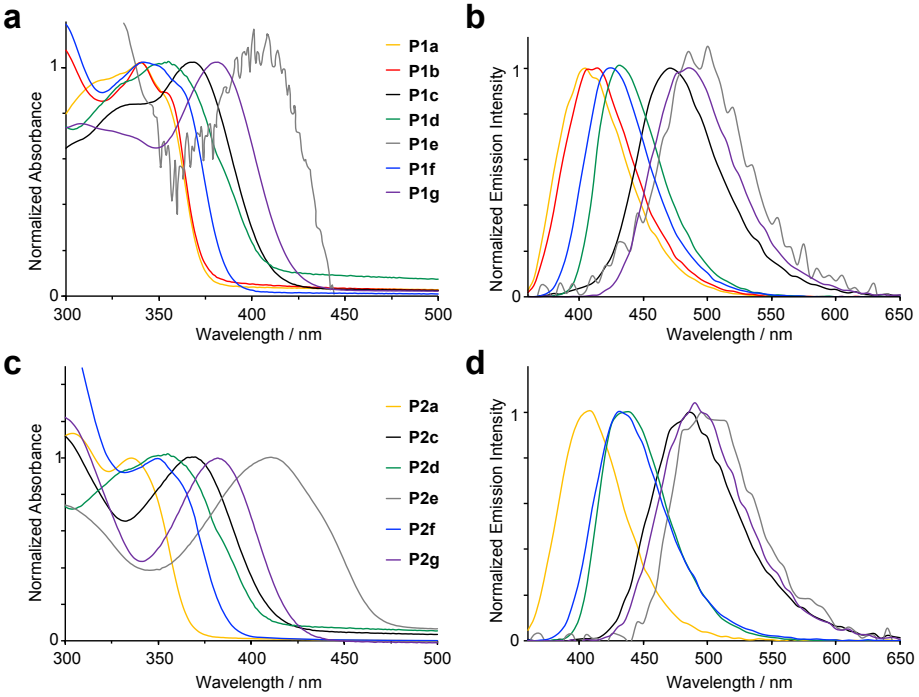

Figure 2. (a) UV-Vis absorption and (b) steady-state emission spectra of **P1a-g**; and (c) UV-Vis absorption and (d) steady-state emission spectra of **P2a-g** in CH_2Cl_2 at 298 K. Molar extinction coefficients (ε / M^{-1} cm^{-1}) are provided in Tables 2 and S1-S4.

Table 2. UV-Vis and photoluminescence properties of **P1-4** in CH_2Cl_2 at 298 K.

Compound	$\lambda_{abs,\,max}$ / nm (ε / M^{-1} cm^{-1})[a]	$\lambda_{em,max}$ / nm (Φ_F / %)[a]	$FWHM_{em}$[b] / cm^{-1}	Stokes shift / cm^{-1} (nm)
P1a	340 (32683)	400 (27)	4874	4412 (60)
P1b	340 (22361)	412 (7)	5652	5140 (72)
P1c	367 (30005)	478 (48)	2073	6327 (111)
P1d	355 (15615)	431 (70)	4046	4888 (75)
P1e	409 (496)	486 (4)	2050	3874 (77)
P1f	342 (34131)	422 (61)	2189	5543 (80)
P1g	381 (71654)	488 (72)	5864	5824 (108)
P2a	336 (56323)	411 (32)	1914	5431 (75)
P2c	370 (22467)	495 (25)	2161	7046 (128)
P2d	355 (15934)	435 (46)	2100	5997 (90)
P2e	410 (35850)	497 (9)	3618	4270 (87)
P2f	349 (13894)	432 (66)	5111	5423 (82)
P2g	382 (16070)	497 (36)	1942	6057 (115)
P3f	354 (32718)	445 (63)	4330	5777 (91)
P3g	385 (68320)	514 (30)	2056	6586 (130)
P4d	356 (20625)	432 (72)	4168	4863 (75)
P4h	367 (8010)	457 (38)	2231	5366 (71)

[a] Fluorescence quantum yield determined relative to quinine sulfate in 0.05 M H_2SO_4 as the standard (Φ_F = 0.52); excitation at λ = 350 nm; entrance/exit slit width = 2 nm. [b] Estimated using an asymmetric pseudo-Voigt fitting function as described in reference[34].

Looking into the influence of substituents, a bathochromic shift in the absorbance maximum is observed when increasingly electron-releasing substituents are introduced at the donor fragment. For example, when the thioether substituent in **P1a** or **P2a** is replaced with stronger amine donors (**P1c**/**P1g**, **P2c**/**P2g**). This is consistent with HOMO destabilization resulting from introduction of the stronger electron-donor moiety.[5] This destabilization is particularly strong when the substituent is *para* to the pyrimidine; only a minor bathochromic shift is observed for **P1f** and **P2f** bearing a 9-ethylcarbazole in which the amine substituent is attached at the *meta* position. A similar dependence on the position of the electron-donor substituent is seen in λ_{max} of **P3f**, which is blue-shifted compared to that of **P3g**. Replacing the thioether donor fragment in **P1a** with a thiophene-derived substituent in **P1b** does not shift the absorbance band maximum, presumably due to the similarity of the Hammett values of methylthioether (0.00) and 2-thiophene (0.05) substituents.[35]

However, increasing the number of linked thiophenes at the donor fragment does induce a significant bathochromic shift (**P1e** and **P2e**) as the stronger electron donating ability of the more electron-rich terthiophene substituent[36] destabilizes the HOMO and contracts the HOMO-LUMO gap. On the other hand, a hypsochromic shift is observed when comparing **P4d** (λ_{max} = 357 nm) and **P4h** (λ_{max} = 367 nm). This suggests that expansion of the aromatic donor fragment, from anthracene to pyrene, leads to HOMO stabilization and a larger HOMO-LUMO gap.

Violet-cyan fluorescence is observed from all 17 pyrimidines (Table 2) with maxima ranging from 400-514 nm and photoluminescence quantum yields of up to 72% measured in CH_2Cl_2 solution at 25 °C. Compared with other D-A-D' and D-A-A pyrimidines,[20,30] the Stokes shifts can be quite narrow (*e.g.*, 60 nm for **P1a**) and the fluorescence quantum yields robust, for example, reaching up to ~70% for **P1d**, **P1g** and **P4d**. Within the library, similar trends are observed in emission as in absorption: strong donors and benzannulation at the donor fragment results in bathochromic and hypsochromic shifts, respectively, in the emission maxima. The most red-shifted emission is seen from **P3g** (λ_{em} = 514 nm), which accordingly exhibits the largest Stokes shift (130 nm). This, however, does not correlate strongly with the emission quantum yield as some of the stronger emitters (Φ_F > 60%; *e.g.*, **P1d**, **P1f**, **P1g**, **P2f**, **P3f** and **P4d**) have variable Stokes shift ranging from 75 nm (**P1d** and **P4d**) to 108 nm (**P1g**). The sulfur-containing compounds **P1a**/**P1b**/**P1e** and **P2a**/**P2e** exhibit the lowest quantum yields, possibly due to competing non-radiative photo-induced electron transfer,[37] though other competing non-radiative pathways are possible. The highest quantum yields (~70%) are generally observed for pyrimidines bearing pyrene, 9-ethylcarbazole, and diphenylamine donors. On the whole, the fluorescence quantum yields measured for this series exceed those reported for similarly fluorescent pyrimidines found in the literature.[4,19,33]

Comparing a representative sample (**P3g**) in its solid form and in dichloromethane solution, a stark change from yellow (solid; Figure S2) to colorless (in solution) can be readily discerned by eye, indicating a sensitivity to the surrounding environment that is consistent with charge-transfer character to its excitation.[38] Air-saturated solutions of **P1c/P1d/P1g**, **P2c/P2d/P2g**, **P3g**, and **P4d** in a variety of solvents were accordingly prepared to investigate the influence of solvent polarity on absorption and emission. In general, bathochromic shifts are observed in both the lowest absorbance band and emission wavelength in solvents of increasing polarity, with the impact on emission more pronounced (Figure 3c-d; Table S1-S4, Figures S3-S17). Interestingly, emission spectra in cyclohexane show vibrational fine structure not apparent in the broader, red-shifted emission in more polar solvents. This is consistent with operation of a locally excited (LE) state in addition to a charge-transfer one in the apolar cyclohexane environment.[39,40] The bathochromic shift observed with increasing solvent polarity and consolidation of the emission peak into a single band indicates the emissive LE state is destabilized relative to the intramolecular charge-transfer state (ICT). These are further accompanied by larger Stokes shifts in solvents of increasing polarity, pointing to significant intra- and intermolecular reorganization to the lowest vibrational state of the emitting excited state. Consistent with these observations, calculated μ_e/μ_g ratios indicate a significant increase in the dipole moment of the excited state (Tables S5-S6).

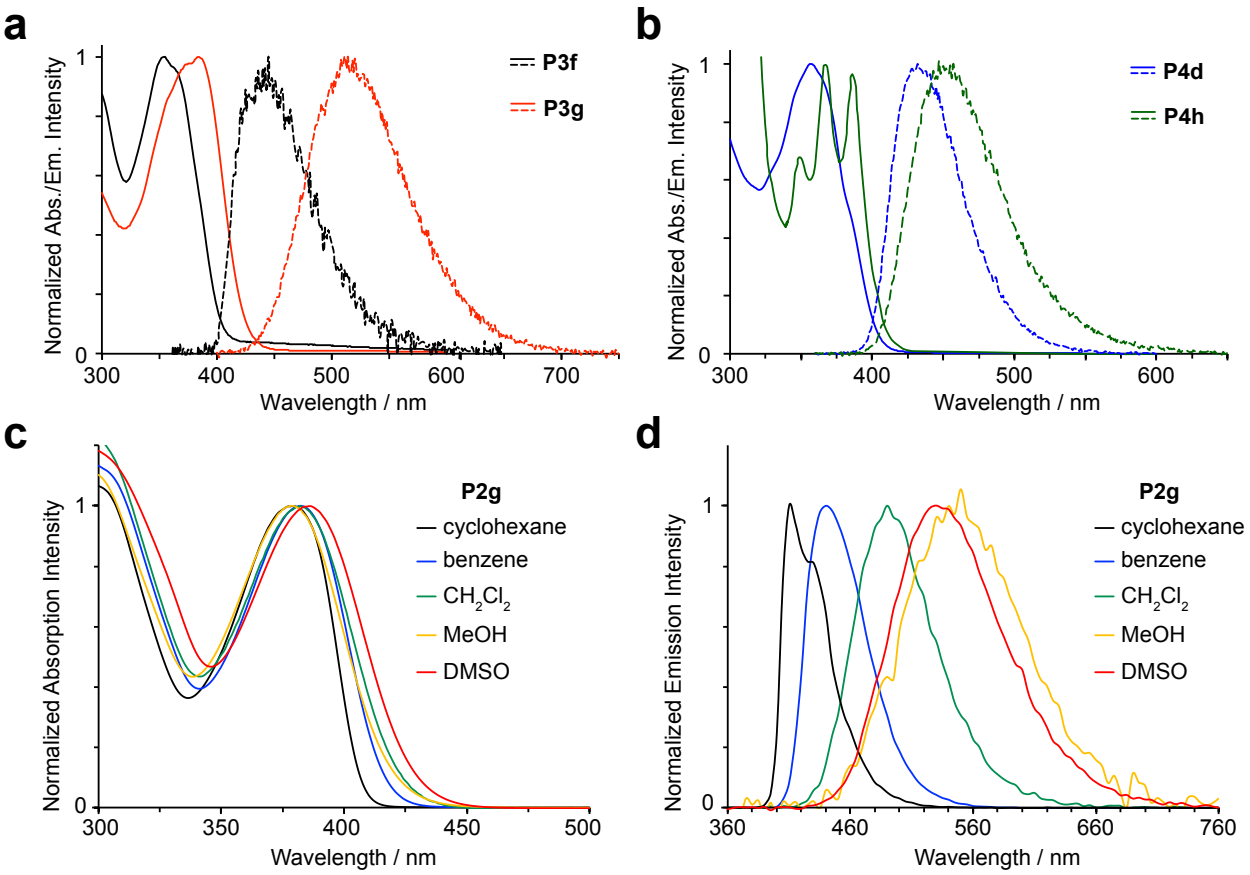

Figure 3. (a) UV-Vis absorbance (solid line) and emission (dashed line) spectra of **P3f** (black) and **P3g** (red) in CH_2Cl_2 solution; (b) UV-Vis absorbance (solid line) and emission (dashed line) spectra of **P4d** (blue) and **P4h** (green) in CH_2Cl_2 solution; (c) UV-Vis absorbance and (d) emission spectra of **P2g** in different solvents. Molar extinction coefficients (ε / M^{-1} cm^{-1}) are provided in Tables 2 and S1-S4.

Electronic Structure Calculations

Density functional theory (DFT) optimizations of pyrimidines **P1c** and **P3g** were carried out to further probe the electronic structures and understand the photophysical properties of two representative pyrimidines. Optimized ground-state bond lengths of the two compounds with

IEFPCM(CH_2Cl_2)-B3LYP-D3(BJ)/6-311G(d,p) show only minor differences compared to the solid-state structures (Figures S18 and S19), though torsional angles about the rotatable single bonds do decrease in the optimized structures of both molecules. The observed flattening of the phenyl and pyrimidine fragment planes appears to be due to an interaction between the C*H*(phenyl) at the *ortho*-position and pyrimidine nitrogen. Other noted differences include an increase to the *p*-orbital character of the dimethylamine nitrogen in **P1c**; the smallest C-N-C angle in the NMe_2 fragment increases from 114.1º in the solid-state structure to 119.0º in the optimized structure, for example. In contrast, there is a slight increase in the torsional angle about the N(diphenyl)-C(phenyl) single bond in the optimized structure of **P3g**, which minimizes intramolecular steric repulsion without affecting the sp^2-hybridization of the diphenylamine nitrogen.

Ground-state frontier molecular orbitals from single point calculations are presented in Figure 4. Isosurfaces of these orbitals suggest D-A-D' (**P1c**) and D-A-A (**P3g**) character, respectively, to the lowest energy absorptions. Consistent with the observed red-shift to the UV-Vis absorbances of **P3g** compared with those of **P1c**, **P3g** has a smaller HOMO-LUMO gap. TDDFT simulated spectra match the experimental spectra of both compounds (Figures S20 and S21). More than one transition contributes to the lowest energy UV-Vis band for both compounds. The strongest transition in **P1c** (Table S7) is nevertheless dominated by a HOMO→LUMO excitation (85%), and has strong CT character as a result. Configuration interaction complicates assignment of the dominant states in **P3g**. Three orbital pairs contribute significantly (contribution > 10%) to the lowest excited state (Table S8). The HOMO→LUMO (45%) and the HOMO→LUMO+1 transition (15%) both present significant electron redistribution, again consistent with CT character. In comparison, the third contributing transition (HOMO-1→LUMO, 24%) has π-π* character localized in the pyrenyl fragment. Overall, this state still largely is CT in

character, consistent with the observed solvatochromism and solvatofluorochromism. In accordance with the orbital character to the HOMO, cyclic voltammograms of both **P1c** and **P3g** show (quasi)reversible oxidations consistent with generation of aminyl radicals (Figure S22, Table S9) that are more reversible for the more sterically protected diphenylamine in **P3g**.

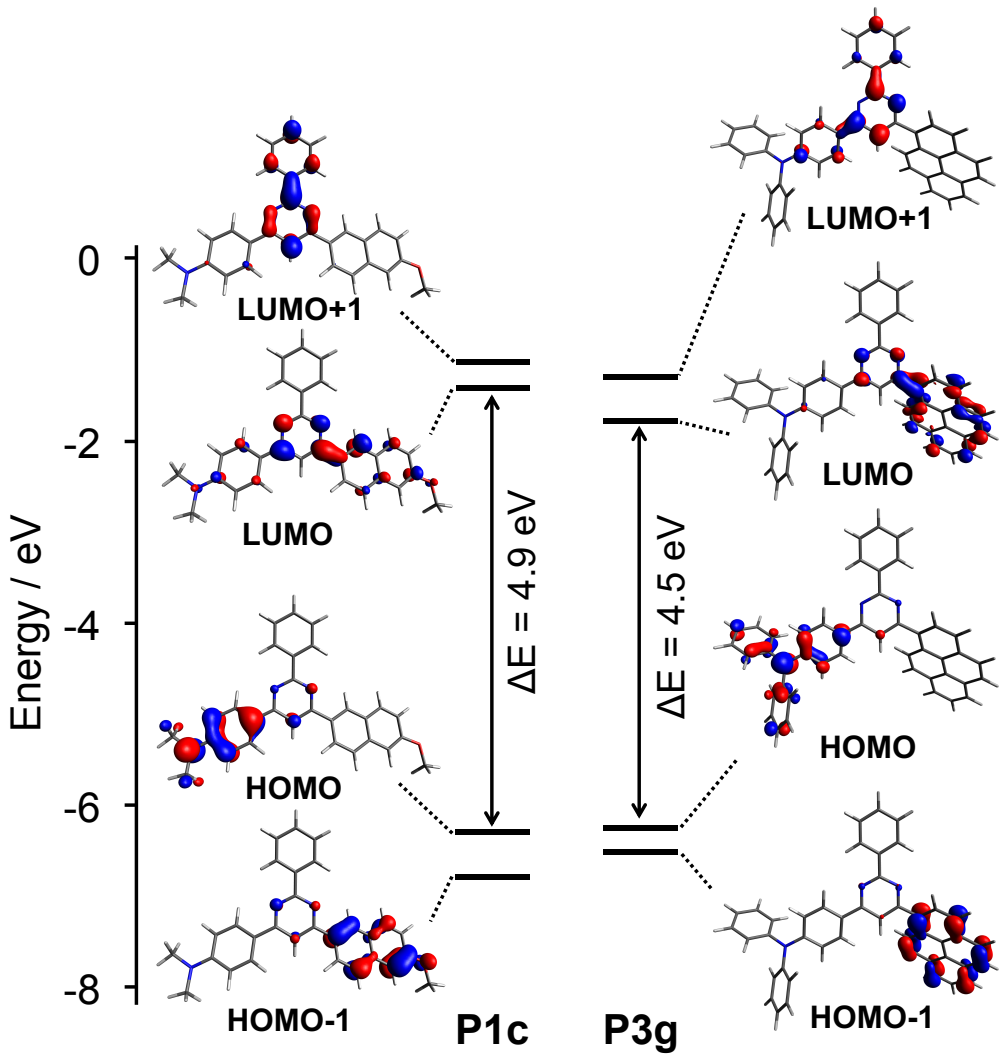

Figure 4. Frontier molecular orbital topologies (IEFPCM-MN15/6-311+G(d,p)//IEFPCM-B3LYP-D3(BJ)/6-311G(d,p); isosurface value = 0.05) of D-A-D' **P1c** and D-A-A **P3g**.

CONCLUSIONS

The synthesis of a novel library of 17 asymmetric D-A-D' and D-A-A luminescent pyrimidines is presented, along with their photophysical characterization. The series of complexes were prepared in one-pot ADC-type reactions using a phenanthridine-based *P^N*-supported Ru complex (**1**), with only water and hydrogen as byproducts. The new pyrimidines absorb to the high energy edge of the visible and emit cyan-violet light with emission wavelength maxima ranging from 400-514 nm, depending on the substitution pattern. With quantum yields measured in solution of up to 72%, and tuneable frontier orbital energies, these emissive materials suggest promising applications in organic optoelectronics. Investigations to this is extent are currently underway.

EXPERIMENTAL DETAILS

General Experimental Information

Air sensitive manipulations were carried out under inert atmosphere in either a glove box (N_2) or using standard Schlenk techniques (Ar). Reactants and reagents used in catalytic reactions were similarly purchased from various chemical vendors as reagent grade or better and used as received (when solids) or stored over dry molecular sieves (when liquids) prior to use. 4-diphenylphosphino-2-methylphenanthridine,[41] **1**,[30] (9-ethyl-9H-carbazol-4-yl)methanol and 4-(diphenylamino)phenyl)methanol,[42] 4-(dimethylamino)phenyl)methanol and 2,2':5',2''-*ter*-thiophene-5-methanol[43] were synthesized following published procedures. Organic solvents were dried over appropriate reagents and deoxygenated prior to use, except for 1,2-dimethoxyethane, water and 2-methoxyethanol, which were simply degassed. NMR spectra (Figures S23-S55) were

recorded on a Bruker Avance 300 MHz or Bruker Avance-III 500 MHz spectrometer as noted. High-resolution mass spectra (Figures S56-S72) were collected using a Bruker microOTOF-QIII.

Solution samples for absorption and emission spectroscopies were prepared under ambient, oxygen saturated conditions in CH_2Cl_2 in 10 x 10 mm^2 quartz cuvettes. Solvatochromism and solvatofluorochromism were examined by dissolving **P1c/P1d/P1g**, **P2c/P2d/P2g**, **P3g**, and **P4d** in different solvents of increasing polarity: cyclohexane, benzene, THF, CH_2Cl_2, MeOH, CH_3CN, and DMSO. Absorbance and emission spectra were collected on a Cary 5000 UV-Vis NIR spectrophotometer and a PTI QM30 fluorimeter (2 nm slit widths, λ_{exc} = 350 nm). Fluorescence quantum yields were measured using quinine sulfate as standard. The FWHM of the fluorescence peaks were estimated using an asymmetric fitting function.[34] All calculations were carried out using Gaussian 16, Rev. B.01.[44] Solvent effects, using CH_2Cl_2, were included implicitly using IEFPCM.[45] Intramolecular interactions were accounted for using Grimme's D3 empirical dispersion with Becke-Johnson damping.[46] Structures for **P1c** and **P3g** were optimized using the B3LYP functional[47,48] and 6-311G(d,p) basis set on all atoms.[49] The B3LYP functional has been shown previously to reproduce the solid-state structures of similar pyrimidine compounds.[19] The MN15 functional[50] with 6-311+G(d,p) basis set[49,51] for all atoms were used to accurately estimate the first 50 vertical excitation energies within the time-dependent DFT (TDDFT) formalism, which should be enough to cover the 300-600 nm range of the spectrum. Functionals with large amounts of HF especially in the long range have been proposed to accurately estimate charge transfer transition energies.[52] Optical spectra were simulated using the GaussSum software package.[53] All structures and molecular orbitals (MOs) were generated with Avogadro.[54]

Synthesis and Characterization of Pyrimidines

General Procedure: A 50 mL Schlenk flask was charged with benzamidine hydrochloride (0.156 g, 1.00 mmol), KO*t*Bu (0.280 g, 2.50 mmol) and dry toluene (3 mL) inside an N_2-filled glove box and the mixture stirred for 15 min. Subsequently, a primary alcohol (1.10 mmol), secondary alcohol (2.00 mmol) and **1** (0.004 g, 0.005 mmol; 0.5 mol %) were added, followed by an additional 5 mL of toluene. The flask was then removed from the glove box, connected to a condenser under Ar atmosphere, and heated to reflux as an open system in an oil bath set heated to 130 °C. After 24 h, the mixture was cooled and filtered through a short plug of silica (~ 1 cm) using CH_2Cl_2-hexanes. Isolated yields are reported following column chromatography on silica.

4-(6-methoxynaphtalen-2-yl)-6-(4-methylthio)phenyl)-2-phenylpyrimidine (P1a): The silica column was performed using CH_2Cl_2/hexanes 7:3 (R_f = 0.80). Yellow solid. Isolated yield = 0.143 g (33 %). ^{1}H NMR ($CDCl_3$, 300 MHz, 22 °C): δ 8.76-8.73 (m, 2H), 8.68 (s, 1H), 8.36-8.33 (m, 1H), 8.26-8.23 (m, 2H), 8.04 (s, 1H), 7.93-7.86 (m, 2H), 7.57-7.55 (overlapped m, 3H), 7.42-7.39 (m, 2H), 7.24-7.19 (m, 2H), 3.96 (s, 3H), 2.57 ppm (s, 3H). ^{13}C{^{1}H} NMR (CD_2Cl_2, 75 MHz, 22 °C): δ 164.6, 164.5, 163.9, 158.9, 142.4, 138.4, 136.2, 134.1, 132.7, 130.7, 128.8, 128.6, 127.7, 127.5, 127.3, 126.1, 124.9, 119.6, 109.6, 105.8, 55.5, 15.4 ppm. HR-MS(ESI+) m/z calcd. For $[C_{28}H_{22}N_2OS+H]^+$ 435.1526, found 435.1501.

4-(6-methoxynaphtalen-2-yl)-2-phenyl-6-(thiophen-2-yl)pyrimidine (P1b): The silica column was performed using CH_2Cl_2/hexanes 1:1 (R_f = 0.60). White solid. Isolated yield = 0.142 g (36 %). ^{1}H NMR (CD_2Cl_2, 300 MHz, 22 °C): δ 8.71-8.68 (overlapped m, 3H), 8.36-8.33 (m, 1H), 7.99-7.89 (overlapped m, 4H), 7.60-7.55 (overlapped m, 4H), 7.25-7.20 (overlapped m, 3H), 3.94 ppm (s, 3H). ^{13}C{^{1}H} NMR ($CDCl_3$, 75 MHz, 22 °C): δ 164.9, 164.7, 160.1, 159.5, 144.0, 138.4, 136.7,

132.8, 131.3, 131.1, 130.4, 129.2, 128.9, 128.8, 127.9, 127.7, 125.2, 120.0, 108.7, 106.2, 55.9 ppm. HR-MS(ESI+) m/z calcd. For $[C_{25}H_{18}N_2OS+H]^+$ 395.1213, found 395.1194.

***N,N*-Dimethyl-4-[6-(methoxynaphalen-2-yl)-2-phenyl-4-pyrimidinyl]benzenamine (P1c):** The silica column was performed using CH_2Cl_2/hexanes 9:1 (R_f = 0.64). Light yellow solid. Isolated yield = 0.129 g (30 %). ^{1}H NMR ($CDCl_3$, 500 MHz, 22 °C): δ 8.78 (m, 2H), 8.69 (s, 1H), 8.35 (m, 1H), 8.27 (m, 2H), 8.00 (s, 1H), 7.93-7.87 (m, 2 H), 7.59-7.51 (m, 3H), 7.23-7.19 (m, 2H), 6.83 (m, 2H), 3.96 (s, 3H), 3.07 ppm (s, 6H). ^{13}C{^{1}H} NMR ($CDCl_3$, 126 MHz, 22 °C): δ 164.5, 164.3, 163.9, 158.8, 152.4, 138.9, 136.0, 133.3, 130.7, 130.4, 128.9, 128.6, 128.5, 128.4, 127.4, 127.1, 125.0, 124.9, 119.5, 111.9, 108.5, 105.9, 55.5, 40.3 ppm. HR-MS(ESI+) m/z calcd. For $[C_{29}H_{25}N_3O+H]^+$ 432.2070, found 432.2073.

4-(6-methoxynaphtalen-2-yl)-2-phenyl-6-(pyren-1-yl)pyrimidine (P1d): The silica column was performed using CH_2Cl_2/hexanes 3:7 (R_f = 0.64). White solid. Isolated yield: 0.158 g (31 %). ^{1}H NMR ($CDCl_3$, 500 MHz, 22 °C): δ 8.82-8.80 (m, 2H), 8.78 (s, 1H), 8.72 (d, J_{HH} = 10 Hz, 1H), 8.45-8.43 (m, 1H), 8.39-8.33 (m, 2H), 8.27-8.24 (m, 2H), 8.19-8.15 (overlapped m, 4H), 8.07 (m, J_{HH} = 10 Hz, 1H), 7.94-7.91 (m, 2H), 7.60-7.55 (m, 3H), 7.24-7.22 (m, 2H), 3.98 ppm. (s, 3H). ^{13}C{^{1}H} NMR ($CDCl_3$, 126 MHz, 22 °C): δ 167.8, 164.7, 164.4, 159.1, 138.4, 136.4, 134.1, 132.6, 132.5, 131.5, 131.0, 130.9, 130.8, 129.1, 128.9, 128.8, 128.7, 128.6, 127.7, 127.5, 126.4, 125.9, 125.6, 125.3, 125.0, 124.9, 124.8, 119.7, 115.9, 105.9, 55.6 ppm. HR-MS(ESI+) m/z calcd. For $[C_{37}H_{24}N_2O+H]^+$ 513.1961, found 513.1965.

4-([2,2':5',2"-*ter*thiophen]-5-yl)-6-(6-methoxynaphtalen-2-yl)-2-phenylpyrimidine (P1e): The silica column was performed using CH_2Cl_2/hexanes 1:1 (R_f = 0.60). Yellow solid. Isolated yield = 0.168 g (30 %). ^{1}H NMR ($CDCl_3$, 500 MHz, 22 °C): δ 8.73-8.71 (m, 3H), 8.36-8.34 (m,

1H), 7.94-7.85 (overlapped m, 4H), 7.58-7.53 (m, 3H), 7.28-7.27 (m, 2H), 7.24-7.15 (m, 5H), 7.05 (m, 1H), 3.98 ppm (s, 3H). An informative $^{13}C\{^1H\}$ spectrum could not be obtained due to poor solubility at higher concentrations. HR-MS (ESI+) m/z calcd. For $[C_{33}H_{22}N_2OS_3+H]^+$ 559.0967, found 559.0963.

4-(6-(6-methoxynaphthalen-2-yl)-2-phenylpyrimidin-4-yl)-9-ethyl-9*H*-carbazole (P1f): The silica column was performed using CH_2Cl_2/hexanes 1:1 (R_f = 0.42). White solid. Isolated yield = 0.220 g (45 %). ^1H NMR ($CDCl_3$, 500 MHz, 22 °C): δ 9.08 (s, 1H), 8.84-8.82 (m, 2H), 8.77 (s, 1H), 8.51-8.49 (m, 1H), 8.44-8.42 (m, 1H), 8.31-8.29 (m, 1H), 8.23 (s, 1H), 7.97-7.91 (m, 2H), 7.62-7.53 (m, 5H), 7.47-7.46 (m, 1H), 7.35-7.32 (m, 1H), 7.25- 7.22 (m, 2H), 4.45-4.41 (m, 2H), 3.98 (s, 3H), 1.53-1.49 ppm (m, 3H). $^{13}C\{^1H\}$ NMR ($CDCl_3$, 126 MHz, 22 °C): δ 165.5, 164.6, 164.5, 158.9, 141.9, 140.8, 138.8, 136.2, 133.2, 130.7, 130.6, 128.9, 128.7, 128.6, 127.5, 127.3, 127.3, 126.3, 125.4, 125.1, 123.6, 123.4, 120.9, 119.9, 119.7, 119.6, 109.8, 108.9, 108.8, 105.9, 55.5, 37.9, 14.0 ppm. HR-MS(ESI+) m/z calcd. For $[C_{35}H_{27}N_3O+H]^+$ 506.2227, found 506.2241.

***N,N*-Biphenyl-4-[6-(methoxynaphalen-2-yl)-2-phenyl-4-pyrimidinyl]benzenamine (P1g):** The silica column was performed using CH_2Cl_2/hexanes 6:4 (R_f= 0.56). Light yellow solid. Isolated yield = 0.250 g (45 %). ^1H NMR ($CDCl_3$, 500 MHz, 22 °C): δ 8.77-8.75 (m, 2H), 8.70 (s, 1H), 8.37-8.35 (m, 1H), 8.21-8.19 (m, 2H), 8.02 (s, 1H), 7.92-7.88 (m, 2H), 7.57-7.49 (m, 3H), 7.35-7.32 (m, 4H), 7.24-7.20 (br overlapped m, 8H), 7.14-7.11 (m, 2H), 3.96 ppm (s, 3H). $^{13}C\{^1H\}$ NMR ($CDCl_3$, 126 MHz, 22 °C): δ 164.5, 164.2, 158.9, 150.5, 147.3, 138.6, 136.1, 132.9, 130.7, 130.6, 129.6, 128.9, 128.6, 128.5, 128.4, 127.5, 127.2, 125.4, 124.9, 123.9, 122.3, 119.6, 109.4, 105.9, 55.5 ppm (C_{Me}-H). HR-MS(ESI+) m/z calcd. For $[C_{39}H_{29}N_3O+H]^+$ 556.2383, found 556.2397.

6-(4-methylthiophenyl)-4-(6-[1,1'-biphenyl])-4-yl)-2-phenylpyrimidine (P2a): The silica column was performed using CH_2Cl_2/hexanes 1:1 (R_f = 0.60). Light Yellow Solid. Isolated yield = 0.193 g (45 %). ^{1}H NMR ($CDCl_3$, 500 MHz, 22 °C): δ 8.76-8.74 (m, 2H), 8.32 (m, 2H), 8.22-8.20 (m, 2H), 7.92 (s, 1H), 7.76 (m, 2H), 7.70-7.68 (m, 2H), 7.59-7.55 (m, 3H), 7.52-7.49 (m, 2H), 7.44-7.38 (m, 3H), 2.55 ppm (s, 3H). ^{13}C{^{1}H} NMR ($CDCl_3$, 126 MHz, 22 °C): δ 164.4, 164.2, 163.9, 143.5, 142.5, 140.4, 138.3, 136.4, 133.9, 130.7, 129.0, 128.6, 128.5, 127.9, 127.7, 127.6, 127.5, 127.2, 126.1, 109.5, 15.3 ppm (C_{SMe}-H). HR-MS(ESI+) m/z calcd. For [$C_{29}H_{22}N_2S$+H^+] 431.1576, found 431.1550.

***N,N*-Dimethyl-4-(6-[1,1'-biphenyl])-4-yl)-2-phenylpyrimidin-4-yl)benzamine (P2c):** The silica column was performed using CH_2Cl_2/hexanes 8:2 (R_f = 0.65). Yellow Solid. Isolated yield = 0.196 g (46 %). ^{1}H NMR ($CDCl_3$, 500 MHz, 22 °C): δ 8.73 (m, 2H), 8.36 (m, 2H), 8.27-8.25 (m, 2H), 7.96 (s, 1H), 7.78 (m, 2H), 7.71-7.69 (m, 2H), 7.56-7.48 (m, 5H), 7.42-7.39 (m, 1H), 6.85-6.83 (m, 2H), 3.09 ppm (s, 6H). ^{13}C{^{1}H} NMR ($CDCl_3$, 126 MHz, 22 °C): δ 164.7, 164.4, 163.7, 152.4, 143.3, 140.7, 138.8, 137.1, 130.5, 129.0, 128.6, 128.5, 127.9, 127.8, 127.7, 127.3, 124.9, 112.0, 108.6, 40.3 ppm. HR-MS(ESI+) m/z calcd. For [$C_{30}H_{25}N_3$+H]$^+$ 428.2121, found 428.2110.

Large-scale preparation of P2c: *N,N*-Dimethyl-4-(6-[1,1'-biphenyl])-4-yl)-2-phenylpyrimidin-4-yl)benzamine (**P2c**) was also prepared on a larger (millimolar) scale using benzamidine hydrochloride (0.780 g, 5 mmol), 4-(dimethylamino)phenyl)methanol (0.832 g, 5.5 mmol), 1-(4-biphenylyl)ethanol (1.983 g, 10 mmol) with KO*t*Bu (1.403 g, 12.5 mmol) and **1** (0.025 g, 0.5 mol%). The same protocol was followed for work-up and isolation. Isolated yield = 0.853 g (40 %).

4-(6-[1,1'-biphenyl])-4-yl)-2-phenyl-6-(pyren-1-yl)pyrimidine (P2d): The silica column was performed using CH_2Cl_2/hexanes 1:1 (R_f= 0.44). White solid. Isolated yield = 0.152 g (30 %). ^{1}H NMR ($CDCl_3$, 500 MHz, 22 °C): δ 8.81-8.79 (m, 2H), 8.70 (d, J_{HH} = 10 Hz, 1H), 8.44-8.42 (m, 2H), 8.37-8.32 (m, 2H), 8.27-8.24 (m, 2H), 8.19-8.14 (m, 3H), 8.09 (s, 1H), 8.08-8.05 (m, 1H), 7.81 (m, 2H), 7.70 (m, 2H), 7.59-7.54 (m, 3H), 7.52-7.49 (m, 2H), 7.43-7.40 ppm (m, 1H). ^{13}C{^{1}H} NMR ($CDCl_3$, 126 MHz, 22 °C): δ 167.9, 164.7, 163.9, 143.9, 140.5, 138.3, 136.3, 133.9, 132.5, 131.5, 131.0, 130.9, 129.1, 128.8, 128.7, 128.0, 127.9, 127.8, 127.7, 127.5, 127.4, 126.4, 125.9, 125.6, 125.3, 125.0, 124.9, 124.8, 116.0 ppm (C_{Ar}H). HR-MS(ESI+) m/z calcd. For $[C_{38}H_{24}N_2+H]^+$ 509.2012, found 509.1990.

4-([2,2':5',2''-terthiophen]-5-yl)-6-(6-[1,1'-biphenyl])-4-yl)-2-phenylpyrimidine (P2e): The silica column was performed using CH_2Cl_2/hexanes 3:2 (R_f = 0.60). Yellow Solid. Isolated yield = 0.177 g (32 %). ^{1}H NMR ($CDCl_3$, 500 MHz, 22 °C): δ 8.70-8.68 (m, 2H), 8.33-8.31 (m, 2H), 7.81 (s, 1H), 7.78-7.76 (m, 3H), 7.69-7.68 (m, 2H), 7.57-7.48 (m, 5H), 7.43-7.40 (m, 1H), 7.23-7.21 (m, 4H), 7.12 (m, 1H), 7.05-7.03 ppm (m, 1H). ^{13}C{^{1}H} NMR ($CDCl_3$, 126 MHz, 22 °C): δ 164.6, 164.1, 159.4, 143.7, 141.9, 141.4, 140.5, 137.9, 137.5, 137.1, 136.3, 135.9, 130.9, 129.1, 128.6, 128.1, 128.1, 128.0, 127.9, 127.8, 127.7, 127.3, 125.4, 124.9, 124.7, 124.6, 124.5 ppm (C_{Ar}H). HR-MS(ESI+) m/z calcd. For $[C_{34}H_{22}N_2S_3+H]^+$ 555.1018, found 555.1028.

4-(6-[1,1'-biphenyl])-4-yl)-2-phenylpyrimidin-4-yl)-9-ethyl-9*H*-carbazole (P2f): The silica column was performed using CH_2Cl_2/hexanes 8:2 (R_f= 0.89). White solid. Isolated yield = 0.251 g (50 %). ^{1}H NMR ($CDCl_3$, 500 MHz, 22 °C): δ 9.02 (s, 1H), 8.84-8.82 (m, 2H), 8.46-8.44 (m, 1H), 8.40 (m, 2H), 8.30-8.28 (m, 1H), 8.09 (s, 1H), 7.81-7.79 (m, 2H), 7.72 (m, 2H), 7.64-7.44 (m, 9H), 7.37-7.34 (m, 1H), 4.38-4.34 (m, 2H), 1.48-1.45 ppm (m, 3H). ^{13}C{^{1}H} NMR ($CDCl_3$, 126 MHz, 22 °C): δ 165.3, 164.3, 163.8, 143.3, 141.7, 140.6, 140.5, 138.6, 136.7, 130.6, 129.0,

128.6, 128.5, 128.2, 127.9, 127.8, 127.6, 127.3, 126.2, 125.2, 123.4, 123.3, 120.9, 119.8, 119.6, 109.6, 108.9, 108.7, 37.8, 13.9 ppm (C_{ethyl}-CH_3). HR-MS(ESI+) m/z calcd. For $[C_{36}H_{27}N_3+H]^+$ 502.2278, found 502.2247.

***N,N*-Biphenyl-4-(6-[1,1'-biphenyl])-4-yl)-2-phenylpyrimidin-4-yl)benzamine (P2g):** The silica column was performed using CH_2Cl_2/hexanes 1:1 (R_f= 0.50). White solid. Isolated yield = 0.237 g (43 %). ^{1}H NMR ($CDCl_3$, 500 MHz, 22 °C): δ 8.75-8.73 (m, 2H), 8.37-8.36 (m, 2H), 8.20-8.18 (m, 2H), 7.97 (s, 1H), 7.80-7.78 (m, 2H), 7.71-7.69 (m, 2H), 7.56-7.48 (m, 5H), 7.42-7.40 (m, 1H), 7.35-7.32 (m, 4H), 7.21-7.20 (m, 6H), 7.14-7.11 ppm (m, 2H). ^{13}C{^{1}H} NMR ($CDCl_3$, 126 MHz, 22 °C): δ 164.5, 164.3, 164.1, 150.6, 147.3, 143.6, 140.5, 138.5, 136.7, 130.7, 130.6, 129.6, 129.1, 128.6, 128.5, 128.4, 127.9, 127.8, 127.7, 127.3, 125.4, 124.0, 122.2, 109.4 ppm. HR-MS(ESI+) m/z calcd. For $[C_{40}H_{29}N_3+H]^+$ 552.2434, found 552.2429.

4-(-2-phenylpyrimidin-4-yl)-6-(pyren-1-yl)9-ethyl-9*H*-carbazole (P3f): The silica column was performed using CH_2Cl_2/hexanes 1:1 (R_f = 0.71). Yellow solid. Isolated yield = 0.236 g (43 %). ^{1}H NMR ($CDCl_3$, 500 MHz, 22 °C): δ 9.11 (m, 1H), 8.83 (m, 1H), 8.74 (m, 1H, $^3J_{HH}$ = 10 Hz), 8.54-8.52 (m, 1H), 8.41-8.39 (m, 1H), 8.35-8.33 (m, 1H), 8.27-8.24 (m, 3H), 8.19-8.15 (overlapped m, 4H), 8.08-8.05 (m, 1H), 7.61-7.52 (m, 5H), 7.48-7.46 (m, 1H), 7.33-7.30 (m, 1H), 4.46-4.42 (m, 2H), 1.52-1.49 ppm (m, 3H). ^{13}C{^{1}H} NMR ($CDCl_3$, 126 MHz, 22 °C): δ 167.5, 165.1, 164.6, 141.9, 140.8, 138.6, 134.4, 132.4, 131.5, 131.1, 130.7, 129.1, 128.8, 128.7, 128.6, 128.2, 127.7, 127.6, 126.4, 126.3, 125.8, 125.5, 125.4, 125.3, 125.0, 124.9, 124.9, 123.7, 123.4, 120.9, 120.1, 119.7, 115.6, 109.0, 108.9, 37.9, 14.0 ppm. HR-MS(ESI+) m/z calcd. For $[C_{40}H_{27}N_3+H]^+$ 550.2278, found 550.2273.

***N,N*-Biphenyl-6-(pyren-1-yl)-2-phenyl-4-pyrimidinyl]benzenamine (P3g):** The silica column was performed using CH_2Cl_2/hexanes 3:2 (R_f = 0.67). Yellow Solid. Isolated yield = 0.233 g (39 %). ^{1}H NMR ($CDCl_3$, 500 MHz, 22 °C): δ 8.77-8.75 (m, 2H), 8.69-8.67 (m, 1H, $^3J_{HH}$ = 10 Hz), 8.35-8.30 (m, 2H), 8.26-8.21 (m, 4H), 8.17-8.13 (m, 3H), 8.07-8.04 (m, 1H), 7.96 (s, 1H), 7.56-7.51 (m, 3H), 7.35-7.31 (m, 4H), 7.21-7.20 (m, 6H), 7.14-7.11 ppm (m, 2H). ^{13}C{^{1}H} NMR ($CDCl_3$, 126 MHz, 22 °C): δ 167.5, 164.5, 163.8, 150.7, 147.2, 138.4, 134.2, 132.4, 131.5, 131.0, 130.8, 130.2, 129.6, 129.0, 128.7, 128.6, 128.5, 128.4, 127.6, 127.5, 126.4, 125.8, 125.5, 125.3, 125.0, 124.9, 124.8, 124.1, 122.1, 115.2 ppm (C_{Ar}). HR-MS(ESI+) m/z calcd. For $[C_{44}H_{29}N_3+H]^+$ 600.2434, found 600.2420.

2,4-diphenyl-6-(pyren-1-yl)pyrimidine (P4d): The silica column was performed using CH_2Cl_2/hexanes 1:1 (R_f = 0.61). Light yellow solid. Isolated yield = 0.160 g (37 %). ^{1}H NMR ($CDCl_3$, 500 MHz, 22 °C): δ 8.83-8.81 (m, 2H), 8.70-8.68 (d, 1H), 8.37-8.35 (m, 2H), 8.33 (s, 1H), 8.31-8.29 (m, 1H), 8.26-8.22 (m, 2H), 8.17-8.12 (m, 3H), 8.07-8.04 (overlapped m, 2H), 7.61-7.56 ppm (m, 3H). ^{13}C{^{1}H} NMR ($CDCl_3$, 126 MHz, 22 °C): δ 167.8, 164.6, 164.3, 138.3, 137.5, 133.9, 132.4, 131.5, 131.0, 130.9, 130.8, 129.1, 129.0, 128.8, 128.7, 128.6, 127.6, 127.5, 127.4, 126.3, 125.9, 125.6, 125.3, 124.9, 124.8, 124.7, 116.0 ppm (C_{Ar}H). HR-MS(ESI+) m/z calcd. For $[C_{30}H_{20}N_2+H]^+$ 433.1699, found 433.1716.

4-(anthracene-9-yl)-6-phenyl-2-(p-tolyl)pyrimidine (P4h): The silica column was performed using CH_2Cl_2/hexanes 1:1 (R_f = 0.60). Yellow solid. Isolated yield = 0.139 g (33 %). ^{1}H NMR ($CDCl_3$, 500 MHz, 22 °C): δ 8.61-8.58 (m, 3H), 8.32 (br m, 2H), 8.11-8.09 (m, 2H), 7.83-7.80 (overlapped m, 3H), 7.55 (m, 3H), 7.51-7.49 (m, 2H), 7.43-7.40 (m, 2H), 7.31 (m, 2H), 2.44 ppm (s, 3H). ^{13}C{^{1}H} NMR ($CDCl_3$, 126 MHz, 22 °C): δ 167.2, 165.3, 164.1, 141.2, 137.3, 135.5,

133.6, 131.6, 131.1, 129.7, 129.4, 129.1, 128.8, 128.7, 128.4, 127.5, 126.5, 125.9, 125.5, 117.4, 21.7 ppm (C_{Me}-H). HR-MS(ESI+) m/z calcd. For $[C_{31}H_{22}N_2+H]^+$ 423.1856, found 423.1838.

X-ray Crystallography

X-ray crystal structure data were collected from multi-faceted crystals of suitable size and quality selected from a representative sample of crystals of the same habit using an optical microscope. In each case, crystals were mounted on MiTiGen loops with data collection carried out in a cold stream of nitrogen (150 K; Bruker D8 QUEST ECO; Mo K_α radiation). All diffractometer manipulations were carried out using Bruker APEX3 software.[55] Structure solution and refinement was carried out using XS, XT and XL software, embedded within the Bruker SHELXTL suite.[56] For each structure, the absence of additional symmetry was confirmed using ADDSYM incorporated in the PLATON program.[57] CCDC Nos. 2018078-2018079 contain the supplementary crystallographic data for this paper. The data can be obtained free of charge from The Cambridge Crystallographic Data Centre via www.ccdc.cam.ac.uk/structures.

Crystal structure data for **P1c** (CCDC No. 2018078): X-ray quality crystals were grown after 3 days at -10 °C from a solution of the compound in a mixture of acetone and pentane. Crystal structure parameters: $C_{29}H_{25}N_3O$ 431.52 g/mol, monoclinic, space group $P2_1/c$; a = 9.5603(5) Å, b = 15.4396(7) Å, c = 14.7968(7) Å, α = 90°, β = 92.646(2)°, γ = 90°, V = 2181.79(18) Å^3; Z = 2, ρ_{calcd} = 1.314 g cm^{-3}; crystal dimensions 0.44 x 0.27 x 0.18 mm^3; θ_{max} = 33.222°; 76282 reflections, 8105 independent (R_{int} = 0.0544), direct methods; absorption coeff (μ = 0.081 mm^{-1}), absorption correction semi-empirical from equivalents (SADABS); refinement (against F_o^2) with SHELXTL V6.1, 301 parameters, 0 restraints, R_1 = 0.0661 ($I > 2\sigma$) and wR_2 = 0.1665 (all data), Goof = 1.029, residual electron density 0.462 and -0.258 e Å^{-3}.

Crystal structure data for **P3g** (CCDC No. 2018079): X-ray quality crystals were grown over two days at -10 °C from a solution of compound dissolved in a mixture of acetone and pentane. Crystal structure parameters: $C_{44}H_{29}N_3$ 599.70 g/mol, triclinic, space group *P*-1; a = 11.7391(6) Å, b = 12.2007(7) Å, c = 13.0911(7) Å, α = 102.3551(18)°, β = 103.2875(18)°, γ = 104.9579(18)°, V = 1686.84(16) $Å^3$; Z = 2, ρ_{calcd} = 1.181 g cm^{-3}; crystal dimensions 0.270 x 0.235 x 0.215 mm^3 ; θ_{max} = 27.548°; 46030 reflections, 7737 independent (R_{int} = 0.0457), direct methods; absorption coeff (μ = 0.069 mm^{-1}), absorption correction semi-empirical from equivalents (SADABS); refinement (against F_o^2) with SHELXTL V6.1, 424 parameters, 0 restraints, R_1 = 0.0610 ($I > 2\sigma$) and wR_2 = 0.1469 (all data), Goof = 1.035, residual electron density 0.298 and -0.343 e $Å^{-3}$.

ASSOCIATED CONTENT

Supporting Information. Additional UV-Vis absorption and emission spectra; computational data tables; cyclic voltammograms; multi-nuclear NMR and HR-MS spectra of all new compounds; crystallographic information files containing all X-ray data. CCDC 2018078-2018079 contain the supplementary crystallographic data for this paper. The data can be obtained free of charge from The Cambridge Crystallographic Data Center via www.ccdc.cam.ac.uk/structures.

The following files are available free of charge:

Supporting Information File (PDF)

Combined Crystallographic Information File (CIF)

AUTHOR INFORMATION

Corresponding Author

David E. Herbert (david.herbert@umanitoba.ca)

ORCIDs

Rajarshi Mondal: 0000-0002-6819-6690

Issiah B. Lozada: 0000-0002-1689-2918

Olha Stotska: 0000-0003-3689-4758

David E. Herbert: 0000-0001-8190-2468

Author Contributions

The manuscript was written through contributions of all authors. All authors have given approval to the final version of the manuscript.

Conflicts of Interest

There are no conflicts of interest to declare.

ACKNOWLEDGMENTS

The following sources of funding are gratefully acknowledged: Natural Sciences Engineering Research Council of Canada for a Discovery Grant to DEH (RGPIN-2014-03733); the Canadian Foundation for Innovation and Research Manitoba for an award in support of an X-ray diffractometer (CFI #32146); the University of Manitoba for the Bert & Lee Friesen Graduate Scholarship (IBL); Mitacs for a Globalink Research Award (OS); and Compute Canada for access to computational resources.

REFERENCES

(1) Johnson, T. B.; Hahn, D. A. Pyrimidines: Their Amino and Aminoöxy Derivatives. *Chem. Rev.* **1933**, *13*, 193–303.

(2) Ono, A.; Torigoe, H.; Tanaka, Y.; Okamoto, I. Binding of Metal Ions by Pyrimidine Base Pairs in DNA Duplexes. *Chem. Soc. Rev.* **2011**, *40*, 5855–5866.

(3) Schenone, S.; Radi, M.; Musumeci, F.; Brullo, C.; Botta, M. Biologically Driven Synthesis of Pyrazolo[3,4-d]Pyrimidines as Protein Kinase Inhibitors: An Old Scaffold as a New Tool for Medicinal Chemistry and Chemical Biology Studies. *Chem. Rev.* **2014**, *114*, 7189–7238.

(4) Achelle, S.; Rodriguez-Lopez, J.; Guen, F. R. Photoluminescence Properties of Aryl-, Arylvinyl-, and Arylethynylpyrimidine Derivatives. *ChemistrySelect* **2018**, *3*, 1852–1886.

(5) Bureš, F. Fundamental Aspects of Property Tuning in Push–Pull Molecules. *RSC Adv.* **2014**, *4*, 58826–58851.

(6) Hughes, G.; Wang, C.; Batsanov, A. S.; Fern, M.; Frank, S.; Bryce, M. R.; Perepichka, I. F.; Monkman, A. P.; Lyons, B. P. New Pyrimidine- and Fluorene-Containing Oligo(Arylene)s: Synthesis, Crystal Structures, Optoelectronic Properties and a Theoretical Study. *Org. Biomol. Chem.* **2003**, *1*, 3069–3077.

(7) Berner, D.; Klein, C.; Nazeeruddin, M. K.; De Angelis, F.; Castellani, M.; Bugnon, P.; Scopelliti, R.; Zuppiroli, L.; Graetzel, M. Efficient Blue Light-Emitting Diodes Based on a Classical "Push-Pull" Architecture Molecule 4,4'-Di-(2-(2,5-Dimethoxyphenyl)Ethenyl)-2,2'-Bipyridine. *J. Mater. Chem.* **2006**, *16*, 4468–4474.

(8) Shaker, M.; Lee, J.-H.; Trinh, C. K.; Kim, W.; Lee, K.; Lee, J.-S. A Facile Method to Synthesize [A' (D'AD)$_2$]-Based Push-Pull Small Molecules for Organic Photovoltaics. *RSC Adv.* **2015**, *5*, 66005–66012.

(9) Raheem, A. A.; Kamaraj, S.; Sannasi, V.; Praveen, C. New D-π-A Push-Pull Chromophores as Low Band Gap Molecular Semiconductors for Organic Small Molecule Solar Cell Applications. *Org. Chem. Front.* **2018**, *5*, 777–787.

(10) Song, C.; Wang, Z.; Li, J.; Chen, Y.; Zhao, F.; Zhang, H. Extension of π-Conjugation and Enhancement of Electron-Withdrawing Ability at Terminal Indenedione for A-π-D-π-A Small Molecules for Application in Organic Solar Cells. *Org. Electron.* **2020**, *81*, 105679.

(11) Kumar, C.; Raheem, A. A.; Pandian, K.; Nandakumar, V.; Shanmugam, R.; Praveen, C. Fine-Tuning the Optoelectronic Chattels of Fluoreno-Thiophene Centred Molecular Semiconductors through Symmetric and Asymmetric Push-Pull Switch. *New J. Chem.* **2019**, *43*, 7015–7027.

(12) Schomaker, J. M.; Delia, T. J. Arylation of Halogenated Pyrimidines via a Suzuki Coupling Reaction. *J. Org. Chem.* **2001**, *66*, 7125–7128.

(13) Hockova, D.; Holy, A.; Masojidkova, M.; Votruba, I. An Efficient Synthesis of Cytostatic Mono and Bis-Alkynylpyrimidine Derivatives by the Sonogashira Cross-Coupling Reactions of 2,4-Diamino-6-Iodopyrimidine and 2-Amino-4,6-Dichloropyrimidine. *Tetrahedron* **2004**, *60*, 4983–4987.

(14) Saygili, N.; Batsanov, A. S.; Bryce, M. R. 5-Pyrimidylboronic Acid and 2-Methoxy-5-Pyrimidylboronic Acid: New Heteroarylpyrimidine Derivatives via Suzuki Cross-Coupling Reactions. *Org. Biomol. Chem.* **2004**, *2*, 852–857.

(15) Stanetty, P.; Hattinger, G.; Schnuerch, M.; Mihovilovic, M. D. Novel and Efficient Access to Phenylamino-Pyrimidine Type Protein Kinase C Inhibitors Utilizing a Negishi Cross-Coupling Strategy. *J. Org. Chem.* **2005**, *70*, 5215–5220.

(16) Delia, T. J.; Schomaker, J. M.; Kalinda, A. S. The Synthesis of Substituted Phenylpyrimidines via Suzuki Coupling Reactions. *J. Heterocycl. Chem.* **2006**, *43*, 127–131.

(17) Dufresne, S.; Hanan, G. S.; Skene, W. G. Preparation, Photophysics, and Electrochemistry of Segmented Comonomers Consisting of Thiophene and Pyrimidine Units: New Monomers for Hybrid Copolymers. *J. Phys. Chem. B* **2007**, *111*, 11407–11418.

(18) Kato, S.-I.; Yamada, Y.; Hiyoshi, H.; Umezu, K.; Nakamura, Y. Series of Carbazole–Pyrimidine Conjugates: Syntheses and Electronic, Photophysical, and Electrochemical Properties. *J. Org. Chem.* **2015**, *80*, 9076–9090.

(19) Pérez-Caaveiro, C.; Oliva, M. M.; López Navarrete, J. T.; Pérez Sestelo, J.; Martínez, M. M.; Sarandeses, L. A. Synthesis of D–A–A and D–A–D Pyrimidine π-Systems Using Triorganoindium Reagents: Optical, Vibrational, and Electrochemical Studies. *J. Org. Chem.* **2019**, *84*, 8870–8885.

(20) Mueller, T. J. J.; Braun, R.; Ansorge, M. A Novel Three-Component One-Pot Pyrimidine Synthesis Based Upon a Coupling-Isomerization Sequence. *Org. Lett.* **2000**, *2*, 1967–1970.

(21) Ghosh, U.; Katzenellenbogen, J. A. A Convenient Method for the Preparation of Highly Substituted Pyrimidines: Synthesis of Tri- and Tetra-Substituted Pyrimidines from 1,3-Dicarbonyl Compounds and *N,N,N′*-Tris-(Trimethylsilyl)Amidines. *J. Heterocycl. Chem.* **2002**, *39*, 1101–1104.

(22) Martinez, R.; Ramon, D. J.; Yus, M. $RuCl_2(DMSO)_4$ Catalyzes the Solvent-Free Indirect Friedlaender Synthesis of Polysubstituted Quinolines from Alcohols. *Eur. J. Org. Chem.* **2007**, 1599–1605.

(23) Deibl, N.; Ament, K.; Kempe, R. A Sustainable Multicomponent Pyrimidine Synthesis. *J. Am. Chem. Soc.* **2015**, *137*, 12804–12807.

(24) Mastalir, M.; Glatz, M.; Pittenauer, E.; Allmaier, G.; Kirchner, K. Sustainable Synthesis of Quinolines and Pyrimidines Catalyzed by Manganese PNP Pincer Complexes. *J. Am. Chem. Soc.* **2016**, *138*, 15543–15546.

(25) Deibl, N.; Kempe, R. Manganese-Catalyzed Multicomponent Synthesis of Pyrimidines from Alcohols and Amidines. *Angew. Chem., Int. Ed.* **2017**, *56*, 1663–1666.

(26) Maji, M.; Kundu, S. Cooperative Ruthenium Complex Catalyzed Multicomponent Synthesis of Pyrimidines. *Dalton Trans.* **2019**, *48*, 17479–17487.

(27) Mondal, R.; Sinha, S.; Das, S.; Chakraborty, G.; Paul, N. D. Iron Catalyzed Synthesis of Pyrimidines Under Air. *Adv. Synth. Catal.* **2020**, *362*, 594–600.

(28) Chakraborty, G.; Sikari, R.; Mondal, R.; Mandal, S.; Paul, N. D. Nickel-Catalyzed Synthesis of Pyrimidines via Dehydrogenative Functionalization of Alcohols. *Asian J. Org. Chem.* **2020**, *9*, 431–436.

(29) Sultana Poly, S.; Siddiki, S. M. A. H.; Touchy, A. S.; Ting, K. W.; Toyao, T.; Maeno, Z.; Kanda, Y.; Shimizu, K. Acceptorless Dehydrogenative Synthesis of Pyrimidines from Alcohols and Amidines Catalyzed by Supported Platinum Nanoparticles. *ACS Catal.* **2018**, *8*, 11330–11341.

(30) Mondal, R.; Herbert, D. E. Synthesis of Pyridines, Quinolines, and Pyrimidines via Acceptorless Dehydrogenative Coupling Catalyzed by a Simple Bidentate *P^N* Ligand Supported Ru Complex. *Organometallics* **2020**, *39*, 1310–1317.

(31) Lipunova, G. N.; Nosova, E. V.; Charushin, V. N.; Chupakhin, O. N. Functionalized Quinazolines and Pyrimidines for Optoelectronic Materials. *Curr. Org. Synth.* **2018**, *15*, 793–814.

(32) Jones, R. N. The Ultraviolet Absorption Spectra of Anthracene Derivatives. *Chem. Rev.* **1947**, *41*, 353–371.

(33) Itami, K.; Yamazaki, D.; Yoshida, J. Pyrimidine-Core Extended π-Systems: General Synthesis and Interesting Fluorescent Properties. *J. Am. Chem. Soc.* **2004**, *126*, 15396–15397.

(34) Korepanov, V. I.; Sedlovets, D. M. An Asymmetric Fitting Function for Condensed-Phase Raman Spectroscopy. *Analyst* **2018**, *143*, 2674–2679.

(35) Hansch, C.; Leo, A.; Taft, R. W. A Survey of Hammett Substituent Constants and Resonance and Field Parameters. *Chem. Rev.* **1991**, *91*, 165–195.

(36) Botek, E.; Champagne, B.; Gangopadhyay, P.; Persoons, A.; Verbiest, T. Theoretical Evaluation of the Faraday Effect in Organic Compounds. *Comput. Lett.* **2007**, *3*, 193–200.

(37) Segawa, H.; Takehara, C.; Honda, K.; Shimidzu, T.; Asahi, T.; Mataga, N. Photoinduced Electron-Transfer Reactions of Porphyrin Heteroaggregates: Energy Gap Dependence of an Intradimer Charge Recombination Process. *J. Phys. Chem.* **1992**, *96*, 503–506.

(38) Lever, A. B. P. Charge Transfer Spectra of Transition Metal Complexes. *J. Chem. Educ.* **1974**, *51*, 612.

(39) Safarzadeh-Amiri, A.; Thompson, M.; Krull, U. J. Trans-4-Dimethylamino-4'-(1-Oxobutyl)Stilbene: A New Fluorescent Probe of the Bilayer Lipid Membrane. *J. Photochem. Photobiol. A* **1989**, *47*, 299–308.

(40) Diwu, Z.; Lu, Y.; Zhang, C.; Klaubert, D. H.; Haugland, R. P. Fluorescent Molecular Probes II. The Synthesis, Spectral Properties and Use of Fluorescent Solvatochromic Dapoxyl Dyes. *Photochem. Photobiol.* **1997**, *66*, 424–431.

(41) Mondal, R.; Lozada, I. B.; Davis, R. L.; Williams, J. A. G.; Herbert, D. E. Site-Selective Benzannulation of *N*-Heterocycles in Bidentate Ligands Leads to Blue-Shifted Emission from $[(P\text{^}N)Cu]_2(\mu\text{-}X)_2$ Dimers. *Inorg. Chem.* **2018**, *57*, 4966–4978.

(42) Brunel, F.; Lautard, C.; di Giorgio, C.; Garzino, F.; Raimundo, J.-M.; Bolla, J.-M.; Camplo, M. Antibacterial Activities of Mono-, Di- and Tri-Substituted Triphenylamine-Based Phosphonium Ionic Liquids. *Bioorg. Med. Chem. Lett.* **2018**, *28*, 926–929.

(43) Cheng, J.; Liang, X.; Cao, Y.; Guo, K.; Wong, W.-Y. Aldehyde End-Capped Terthiophene with Aggregation-Induced Emission Characteristics. *Tetrahedron* **2015**, *71*, 5634–5639.

(44) Frisch, M. J.; Trucks, G. W.; Schlegel, H. B.; Scuseria, G. E.; Robb, M. A.; Cheeseman, J. R.; Scalmani, G.; Barone, V.; Petersson, G. A.; Nakatsuji, H.; Li, X.; Caricato, M.; Marenich, A. V.; Bloino, J.; Janesko, B. G.; Gomperts, R.; Mennucci, B.; Hratchian, H. P.; Ortiz, J. V.; Izmaylov, A. F.; Sonnenberg, J. L.; Williams-Young, D.; Ding, F.; Lipparini, F.; Egidi, F.; Goings, J.; Peng, B.; Petrone, A.; Henderson, T.; Ranasinghe, D.; Zakrzewski, V. G.; Gao, J.; Rega, N.; Zheng, G.; Liang, W.; Hada, M.; Ehara, M.; Toyota, K.; Fukuda, R.; Hasegawa, J.; Ishida, M.; Nakajima, T.; Honda, Y.; Kitao, O.; Nakai, H.; Vreven, T.; Throssell, K.; Montgomery, J. A.; Peralta, J. E.; Ogliaro, F.; Bearpark, M. J.; Heyd, J. J.; Brothers, E. N.; Kudin, K. N.; Staroverov, V. N.; Keith, T. A.; Kobayashi, R.; Normand, J.; Raghavachari, K.; Rendell, A. P.; Burant, J. C.; Iyengar, S. S.; Tomasi, J.; Cossi, M.; Millam, J. M.; Klene, M.; Adamo, C.; Cammi, R.; Ochterski, J. W.; Martin, R. L.; Morokuma, K.; Farkas, O.; Foresman, J. B.; Fox, D. J. *Gaussian 16, Revision B.01*; Gaussian 16, Revision B.01, Gaussian, Inc., Wallingford CT; Gaussian, Inc.: Wallingford CT, 2016.

(45) Scalmani, G.; Frisch, M. J. Continuous Surface Charge Polarizable Continuum Models of Solvation. I. General Formalism. *J. Chem. Phys.* **2010**, *132*, 114110/1-114110/15.

(46) Grimme, S.; Ehrlich, S.; Goerigk, L. Effect of the Damping Function in Dispersion Corrected Density Functional Theory. *J. Comput. Chem.* **2011**, *32*, 1456–1465.

(47) Becke, A. D. Density-Functional Exchange-Energy Approximation with Correct Asymptotic Behavior. *Phys. Rev. A* **1988**, *38*, 3098–3100.

(48) Lee, C.; Yang, W.; Parr, R.G. Development of the Colle-Salvetti Correlation-Energy Formula into a Functional of the Electron Density. *Phys. Rev. B Condens. Matter.* **1988**, *37*, 785–789.

(49) Krishnan, R.; Binkley, J. S.; Seeger, R.; Pople, J. A. Self-Consistent Molecular Orbital Methods. XX. A Basis Set for Correlated Wave Functions. *J. Chem. Phys.* **1980**, *72*, 650–654.

(50) Yu, H. S.; He, X.; Li, S. L.; Truhlar, D. G. MN15: A Kohn-Sham Global-Hybrid Exchange-Correlation Density Functional with Broad Accuracy for Multi-Reference and Single-Reference Systems and Noncovalent Interactions. *Chem. Sci.* **2016**, *7*, 5032–5051.

(51) Clark, T.; Chandrasekhar, J.; Spitznagel, G. W.; Schleyer, P. v R. Efficient Diffuse Function-Augmented Basis Sets for Anion Calculations. III. The 3-21 + G Basis Set for First-Row Elements, Lithium to Fluorine. *J. Comput. Chem.* **1983**, *4*, 294–301.

(52) Adamo, C.; Jacquemin, D. The Calculations of Excited-State Properties with Time-Dependent Density Functional Theory. *Chem. Soc. Rev.* **2013**, *42*, 845–856.

(53) O'Boyle, N. M.; Tenderholt, A. L.; Langner, K. M. Software News and Updates Cclib: A Library for Package-Independent Computational Chemistry Algorithms. *J. Comput. Chem.* **2008**, *29*, 839–845.

(54) Hanwell, M. D.; Curtis, D. E.; Lonie, D. C.; Vandermeersch, T.; Zurek, E.; Hutchison, G. R. Avogadro: An Advanced Semantic Chemical Editor, Visualization, and Analysis Platform. *J. Cheminf.* **2012**, *4*, 17.

(55) Bruker-AXS. *APEX3 V2016.1-0*; Madison, Wisconsin, USA, 2016.

(56) Sheldrick, G. M. A Short History of SHELX. *Acta Cryst.* **2008**, *A64*, 112–122.

(57) Spek, A. L. Structure Validation in Chemical Crystallography. *Acta Cryst.* **2009**, *D65*, 148–155.

Table of Contents/Abstract Graphic

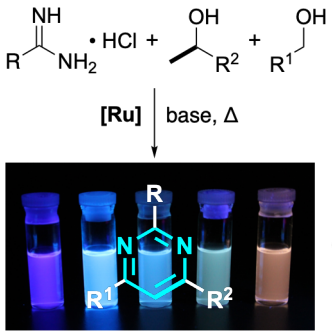

17 Examples

Fluorescence Quantum Yields Up to 72%